Heliyon 10 (2024) e40514

Contents lists available at ScienceDirect

Heliyon

journal homepage: www.cell.com/heliyon

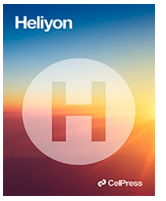

Research article

Effect of annealing temperatures on the properties of CdZrS nanoparticles prepared by sol-gel synthesis method

A.U. Yimamu [a,b], V.N. Adoons [a,*], R.A. Phokojoe [a,c]

[a] Department of Physics, University of the Free State, QwaQwa Campus, Phuthaditjhaba, 9866, South Africa
[b] Department of Physics, Dire Dawa University, Dire Dawa, Ethiopia
[c] Department of Applied Physical Sciences, Vaal University of Technology, Vanderbijl Park, 1900, South Africa

ARTICLE INFO

Keywords:
CdZrS
Alloy
Novel synthesis
Solar energy
Annealing temperature

ABSTRACT

Cadmium zirconium sulphide (CdZrS) nanoparticles (NPs) were prepared using a sol-gel method. The effect of different annealing temperatures on the structural, morphological, optical, and compositional properties of CdZrS NPs was investigated. The structural investigation revealed that the CdZrS samples exhibit hexagonal and cubic structures in both the as-prepared and annealed samples. The crystallite sizes of CdZrS nanoparticles decreased with increasing annealing temperature. The scanning electron microscopy (SEM) images showed a highly agglomerated particle at 500°C. Energy dispersive X-ray spectroscopy (EDS) confirmed the presence of Cd, Zr and S in all samples. UV–Vis analysis confirmed a red shift from 2.61 to 1.62 eV when the annealing temperature was increased. Photoluminescence (PL) emission spectra showed a peak at 462 nm attributed to excitonic recombination of CdZrS and a peak at 557 nm corresponding to interstitial sulfur sites. These materials have potential applications for biosensors or solar cells technology.

1. Introduction

The size confinement effect of semiconductor nanocrystals makes their manufacture and characterization crucial for scientific and practical research due to their tunable electrical, optical, and catalytic properties [1–4]. Group II-IV semiconductor chalcogenide nanomaterials have been used for various applications owing to their energy band gap (1.45–3.62 eV) in the near visible spectral range [5–8]. Because of its wide energy (2.42 eV) and direct band gap, cadmium sulfide (CdS) is one semiconductor photocatalyst that has been the subject of extensive research recently [9]. CdS is among the members of the group, and it is used for sensors [10], humidity sensing [11], bio-imaging [12], solar energy [13], and photoelectrochemical cells applications [7].

To improve the properties of semiconductor materials, various metal dopants are added in different concentrations. The increase in photocatalytic efficiency of CdS nanoparticles is significantly influenced by the creation of sophisticated structures [14]. In order to fulfill the essential function of technologically relevant and cutting-edge research materials such as solar cells, it is possible to dope semiconductor nanocrystals with various transition metals [15–17]. It was found that the electrical and optical properties changed when metals were added to the semiconductor material. An improvement in optical properties was observed when Zr was incorporated into ZnO nanoparticles [18]. The photocatalytic activity of CdO increased with the addition of Zr [19]. When Zr was added to CeO_2 at different concentrations, the energy band gap increased with increasing Zr concentration [20]. A change in the properties of ZnS

* Corresponding author.
E-mail address: adoonsvn@ufs.ac.za (V.N. Adoons).

https://doi.org/10.1016/j.heliyon.2024.e40514
Received 13 August 2024; Received in revised form 28 October 2024; Accepted 18 November 2024
Available online 19 November 2024

nanoparticles was reported after the incorporation of Zr [21]. To improve the properties of CdS semiconductor materials, various metals are used as dopants. In this study, Zr was chosen as an additive (now additive) to CdS due to the free electrons in Zr^{4+}. Zr^{4+} can replace the position of Cd^{2+} because they have an ionic radius of 0.74 and 0.97 Å, respectively [22]. The properties of CdZrS nanoparticles depend on the conditions and techniques used to grow them. Zr was added to form a trinary compound. CdZrS nanoparticles were synthesized because Zr is a corrosion resistant nature and increases the stability and lifespan of the materials. It was reported that doping CdS with Zr caused a blue shift in the optical band gap values, which was explained by the Moss-Burstein effect [5].

According to the CdS structure, Cd^{2+} has two valence electrons, and S^{2-} accepts these two electrons from Cd^{2+} to form an ionic compound. The crystal structure shows a charge carrier gradient because Zr^{4+} donates four electrons, of which S^{2-} needs two to form an ionic bond. This allows two electrons to be released free in the system.There are several approaches for the synthesis of CdZrS. For this study, the sol-gel method was chosen due to its certain advantages over other approaches, such as a wide range of inexpensive precursors, more precise control of phase formation, simple manufacturing process with the required stoichiometry and uniformity in particle size [23,24].

There is limited literature showing studies on the effect of different annealing temperatures for CdZrS NPs. This work investigates the effect of different annealing temperatures on the structural, optical, morphological and compositional properties of CdZrS NPs synthesized by the sol-gel approach, which has not been reported previously.

2. Experimental method

CdZrS NPs were prepared using the sol-gel (novel) method. The solution matrix contained 0.03 M cadmium acetate dihydrate (Cd $(CH_3OO)_2.2H_2O$), 0.005 M zirconium acetate, and 0.003 M Na_2 S_2O_2 sodium thiosulphate in 100 ml deionized water (DW). Sulfuric acid (H_2SO_4) and ammonium hydroxide (NH_4OH) were added as reactants under ambient conditions. What is called novel synthesis, this approach does not use a no complex agent. For the first time, a solution with the same concentration was prepared with 400 ml of DW, and electrodeposition of thin films occurred, which is reported [25]. Then, the next day, the solution began to form a gel. The concentration we prepared for CdZrS is the same, but the DW is reduced due to solution preparation and is not the same as the normal sol-gel approach.

To synthesize the CdZrS powder, 0.03 M Cd $(CH_3OO)_2.2H_2O$ was dissolved in 100 ml DW and stirred for 10 min. The next source is 0.003 M Na_2 S_2O_2, which was added to the solution and stirred for 30 min. Finally, 0.005 M zirconium acetate was added, and the solutions were stirred for 60 min, slowly dissolving. The pH of the solution was increased to 1.85 by using dilute sulfuric acid (H_2SO_4), and ammonium hydroxide (NH_4OH) was added as a reactant under ambient conditions. The solution was stirred at 85 °C for 5 h to reduce the solution water and make it more dissolved. The solution was dried in an oven at a temperature of 70° C for 168 h. The powder was then annealed at intervals of 100 °C at temperatures between 200 and 500 °C. The effect of annealing temperature on the structure, morphology, optical properties, and elemental composition of CdZrS NPs was studied using various techniques such as X-ray diffraction (XRD), UV–vis spectroscopy (UV–Vis), scanning electron microscope (SEM), energy-dispersive X-ray spectroscopy (EDS) and photoluminescence (PL) respectively.

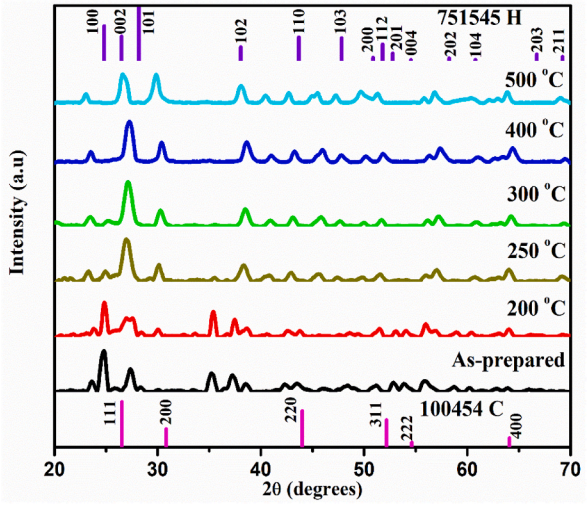

Fig. 1. XRD patterns of the CdZrS NPs both in their initial preparation and following various annealing temperatures.

3. Results and discussion

3.1. Structural properties

Fig. 1 depicts the X-ray diffraction (XRD) patterns of CdZrS NPs and shows cubic CdZrS peaks at $2\theta = 26.52^{o}$, 30.83^{o}, 43.99^{o}, 52.18^{o}, 54.63^{o}, and 64.09^{o} corresponding to (111), (200), (311), (222) and (400) reflections planes, respectively, and hexagonal CdZrS peaks at $2\theta = 24.80^{o}$, 26.49^{o}, 28.17^{o}, 36.60^{o}, 43.67^{o}, 47.81^{o}, 50.87^{o}, 51.87^{o}, 52.78^{o}, 54.55^{o}, 58.26^{o}, 60.80^{o}, 66.74^{o} and 69.43^{o}, corresponds to the planes of (100), (002), (101), (102), (110), (103), (200), (112), (201), (004), (202), (104), (203) and (210) reflections, respectively. The analysis results are in good agreement with the JCPDS cards 20454 and 751545 for cubic and hexagonal CdZrS, respectively. It can be seen that CdZrS samples undergo a structural change from cubic to hexagonal with increasing annealing temperature. The reason for this structural change is that cubic CdZrS is more stable at lower temperatures, while hexagonal CdZrS becomes more favorable at higher temperatures. Reports on the coexistence of cubic and hexagonal phases in the prepared samples have been previously published [24].

The average crystallite size (D) of all samples was computed using the Debye Sheerer's equation [26]:

$$D = \frac{k\,\lambda}{\beta \cos\theta} \tag{1}$$

where β the full width at half maximum (FWHM) of each diffraction peak, k is a constant, taken as 0.9, λ is the wavelength of the X-ray (0.15418 nm), and θ is Bragg's diffraction angle.

The calculated D values were 51, 26, 20, 18, and 15 nm for the as-prepared sample and samples annealed at 200, 300, 400, and 500 °C, respectively. As the annealing temperature increased, the crystallite sizes of the CdZrS NPs decreased. The general trend is that as the annealing temperature increases, the crystallite sizes also increase.

However, in this study, the increase in annealing temperature contradicts this general trend, which is due to the recrystallization process and phase transformation. During recrystallization, new grains or crystallites form, and the initially fine grains can transform into smaller, more uniform grains. As reported above, CdZrS samples undergo phase transformation when the annealing temperature is increased which can result in a more stable phase with a finer grain structure. For example, the transformation from cubic to hexagonal structures may involve growth kinetics that favours smaller grain sizes. The as-prepared sample has the maximum crystallite size due to particle agglomeration. The overall structural analysis shows that as the annealing temperature is increased, the peaks disappeared,

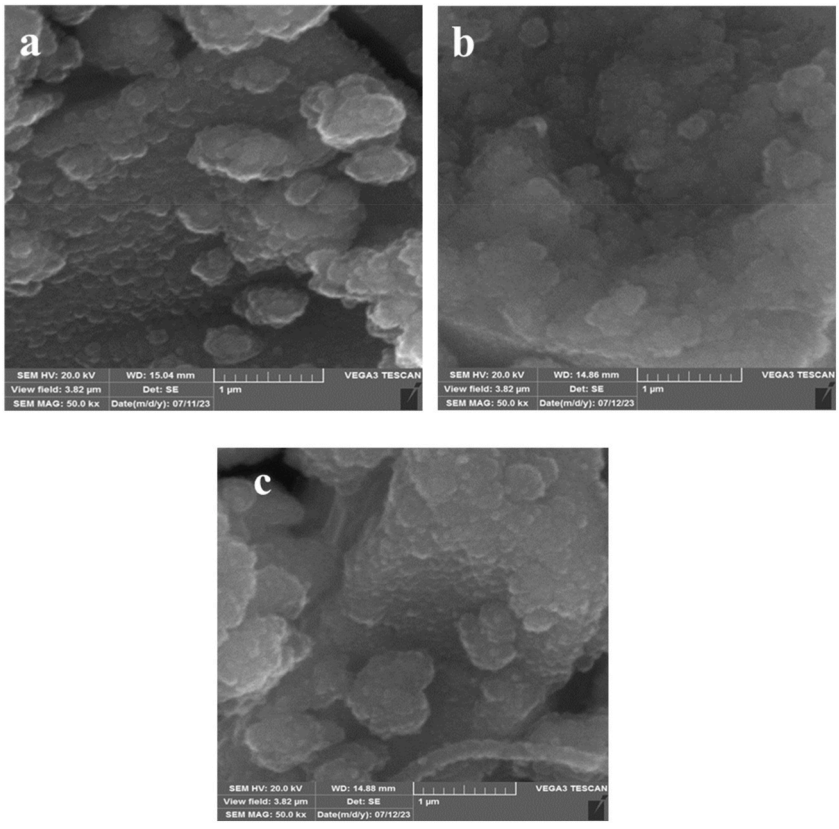

Fig. 2. SEM images of CdZrS nanoparticles annealed at different temperatures: (a) as-prepared (b) 300°C (c) 500°C.

and more visible peaks were observed. The length of the dislocation lines per unit volume, known as the dislocation density (δ) of the formed CdZrS, was calculated using equation (2) [27]. The micro-strain (ε) was estimated using equation (3) [28].

$$\delta = \frac{1}{D^2} \tag{2}$$

$$\varepsilon = \frac{\beta_{hkl}}{4 \tan \theta} \tag{3}$$

The analysis result shows that the dislocation density varied with the annealing temperature and was recorded as 7.91, 2.40, 4.06, 4.52, and 5.45 x 10^{15} lines/m^2 for as-prepared sample and annealed samples, respectively. The microstrain values were reduced from 0.33, 0.64, 0.80, 0.98, and 0.91 x 10^{-2} for as-prepared and annealed samples at 200, 300, 400, and 500 °C, respectively. The as-prepared sample exhibited a high dislocation density of 7.91 × 10^{15} lines/m^2, which decreased to 2.40 × 10^{15} lines/m^2 after annealing at 200 °C, indicating recovery processes. However, the densities increased at 300 °C (4.06 × 10^{15} lines/m^2) and peaked at 500 °C (5.45 × 10^{15} lines/m^2), which is probably due to the formation of new defects by thermal effects. Initially, the microstrain for the as-prepared was 0.33 × 10^{-2}. It increased to 0.64 × 10^{-2} at 200 °C and reached a peak value of 0.98 × 10^{-2} at 400 °C, reflecting persistent internal stresses. A slight decrease to 0.91 × 10^{-2} at 500 °C indicates some recovery, although significant lattice distortion remains.

3.2. Morphology

The surface morphology of the CdZrS nanoparticles was examined using SEM. The development of application in technology requires a fundamental understanding of the surface morphology of the manufactured materials [29]. SEM images of as-prepared sample and annealed samples at temperatures of 300 and 500 °C are shown in Fig. 2(a) and (b) and (c). As shown in Fig. 2, the particles are spherical, but their size decreases with annealing temperature from 300 °C to 500 °C. Although the particles can be distinguished, they are highly agglomerated, causing smaller particles to overlap due to annealing. It is clear that increasing the annealing temperature results in more agglomerated particles. The result confirms that the grain size and shape of the surface morphology changed with the annealing temperature. The reduction in grain size with increasing annealing temperature in CdZrS samples despite initial agglomeration can be attributed to a combination of sintering effects, diffusion processes and phase transformation. While particles are agglomerated, heat treatment of samples facilitates interactions that result in smaller particle sizes, as confirmed by XRD analysis.

3.3. Elemental composition

The element formation of CdZrS samples was analyzed using EDS. EDS shows the presence of Cd, Zr and S and confirms that CdZrS samples contain expected elements and corresponding peaks (see Fig. 3(a) and (b)). The presence of C peaks is related to the carbon tape used during SEM and EDS measurements. The results are in good agreement with previously published results [30]. Fig. 4 shows the colour distribution of Cd, Zr and S in the CdZrS NPs. The result confirmed that the emergence and surface map of each element in the sample.

3.4. UV–vis spectroscopy

The influence of annealing temperature on the optical properties of the CdZrS NPs was studied by UV–Vis. The absorbance and reflectance spectra of the as-prepared CdZrS NPs after annealing are shown in Fig. 5(a) and (b). An observation of the matching absorption edge was made at 435 nm for the as-prepared sample. Due to a change in crystallite size, a slight redshift of the absorption peak occurs in annealed samples. Furthermore, reflectivity increases with annealing temperature (see Fig. 5 (b)). Because the as-prepared sample has a lower absorbance value than annealed samples, it was found that their reflectance values are higher in the visible region.

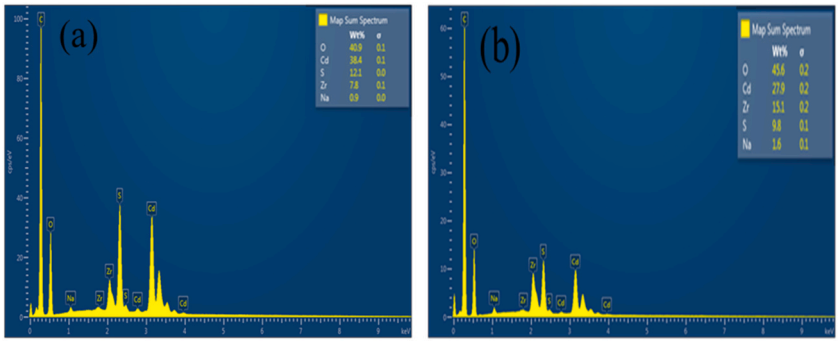

Fig. 3. EDS spectra of CdZrS nanoparticles (a) 300 °C and (b) 500 °C.

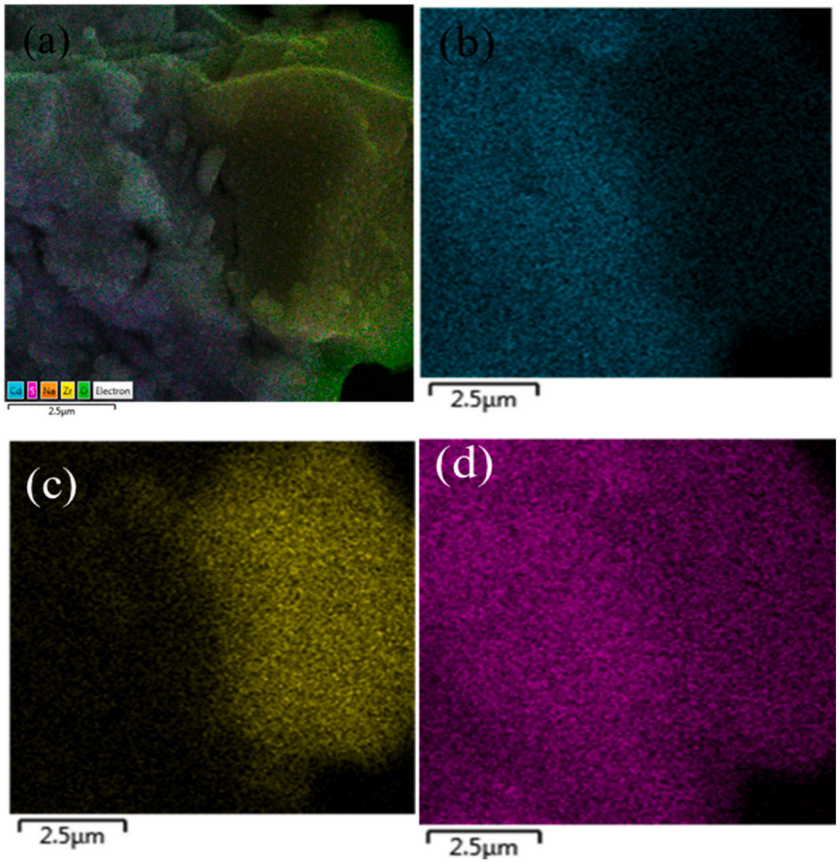

Fig. 4. The colour distribution for representative annealed at 300 °C (a) CdZrS, (b) Cd, (c) Zr, and (d) S.

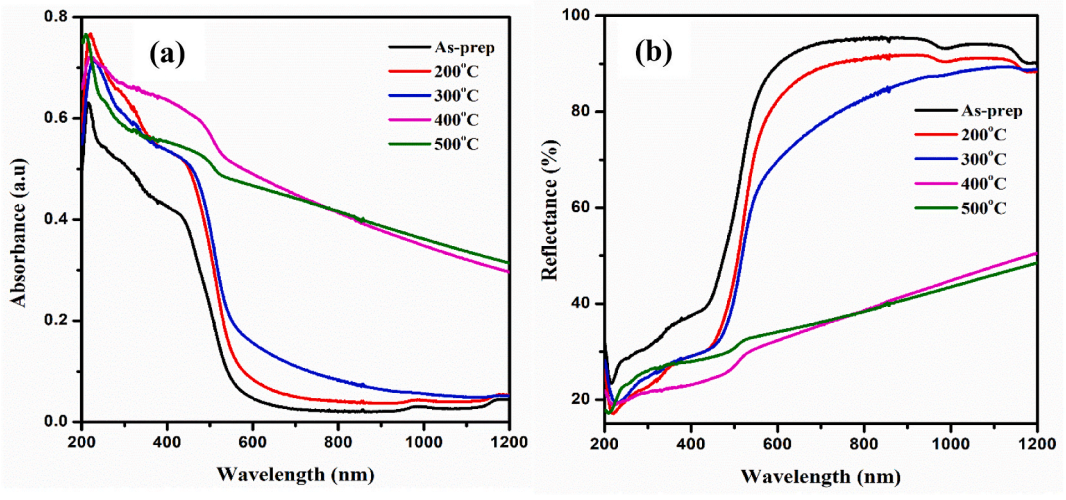

Fig. 5. (a) Absorbance and (b) reflectance spectra of as-prepared CdZrS and sample annealed at different temperatures.

The similarities observed in the UV absorbance and reflectance spectra of hexagonal CdZrS and cubic CdZrS, especially after annealing at 300 °C, can be attributed to several interrelated factors: phase stabilization, improvements in crystallinity and defect density, similarities in electronic band structure and morphological effects that influence optical properties.

The optical band gap energy (*Eg*) of the samples was calculated using the following relationship:

$$\alpha h\nu = A\,(h\nu - Eg)n \tag{4}$$

where α is the absorption coefficient derived from the absorption data, $h\nu$ is the photon energy, *and A* is the constant. The n value depends on the type of transition. n = ½ for direct and 2 for indirect transition. When extrapolating the linear part of the curves, as shown in Fig. 6, the intersection on the energy axis $(\alpha h\nu)^2 = 0$ gives the band gap of the material. The optical band gap showed a shift from 2.61, 2.29, 2.23, 1.76, and 1.62 eV with increasing annealing temperature The reduction of defects, which decreases the S concentration and increases the Cd concentration due to higher annealing temperatures, can lead to a decrease in the band gap energy [31,32]. Ideally, there should be no free electrons or holes in the crystal system because S^{2-} takes over the two valence electrons from Cd^{2+} in the CdS structure to form an ionic compound. On the other hand, Zr^{4+} provides four electrons, of which S^{2-} requires two to form an ionic connection. This releases two electrons in the system, and creates a charge carrier gradient in the crystal structure [5]. The addition of Zr can influence the electronic structure and band gap of CdS, allowing customization of its optical properties to better suit specific applications, such as solar cells. The challenge with CdS window materials is absorption loss. Zr can help passivate surface defects, reduce non-radiative recombination, and increase the efficiency of charge carriers [33].

3.5. Photoluminescence spectroscopy

The PL spectra in Fig. 7(a) show the emissions of the CdZrS NPs upon excited with an excitation wavelength of 271 nm. The as-prepared CdZrS sample shows a broad emission peak at 557 nm (2.23 eV) and a shoulder peak at 462 nm (2.68 eV). The peak at 557 nm is attributed to interstitial sulfur sites [34,35]. The 462 nm peak is attributed to the excitonic recombination of CdS [34]. The band-edge emission peak (462 nm) is visible in all air-annealed samples. This is due to the elimination of defects during annealing [36]. According to Gemain et al. [34], an annealing environment in oxygen induces the replacement of sulfur interstitial sites with oxygen. The PL intensity of the emission spectra increases with annealing temperature up to 300 °C and eventually decreases as the annealing temperature is further increased. This could be due to the saturation of oxygen vacancies created by localized excitons [37]. The International Commission on Illumination (C.I.E.) colour chromaticity diagram for the CdZrS samples is shown in Fig. 6 (b). The C.I.E. colour coordinates of the samples are listed in Table 1. The C.I.E. colour position of the as-prepared CdZrS sample is light blue-green, and all the annealed samples are clustered in the green-blue region. This shows that annealing affects the emission colour of CdZrS.

4. Conclusions

In this study, CdZrS NPs were successfully synthesized using a low-cost sol-gel approach. The investigation focused on how annealing temperatures influence the properties of the CdZrS nanomaterials. Structural analysis showed that the crystallite sizes of annealed CdZrS samples decreased with increasing annealing temperature, which is attributed to the recrystallization process. Furthermore, XRD analysis showed that the as-prepared and annealed CdZrS samples exhibited both cubic and hexagonal structures. SEM images show that the particles of the as-prepared sample are spherical and are highly agglomerated at 500 °C. EDS confirmed the presence of Cd, Zr, and S in all samples. UV–Vis absorption spectra of the annealed CdZrS samples showed a shift in the absorption peak and a decrease in the band gap energies with absorbance spectra of the annealed material. This is explained by larger crystallite sizes caused by higher annealing temperatures. The PL results show that as the annealing temperature increases, the emission intensity increases up to 300 °C and then decreases with further annealing. This is due to the saturation of oxygen vacancies created by localized excitons. Zr doping can significantly improve the performance and applicability of CdS nanoparticles in various fields, including energy conversion and environmental remediation. The results of this study serve as a basis for further investigations into the optimization of CdZrS nanomaterials for optoelectronic and photovoltaics applications. Our future recommendation will be that device fabrication and computational studies are possible to obtain a comprehensive understanding of the electronic structure and exciton

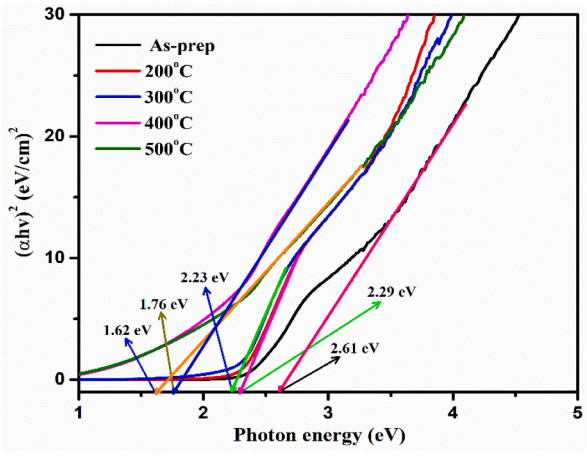

Fig. 6. Plot of the linear portion of $(\alpha h\nu)^2$ against the photon energy of the as-prepared CdZrS sample and after annealing the sample at indicated temperatures.

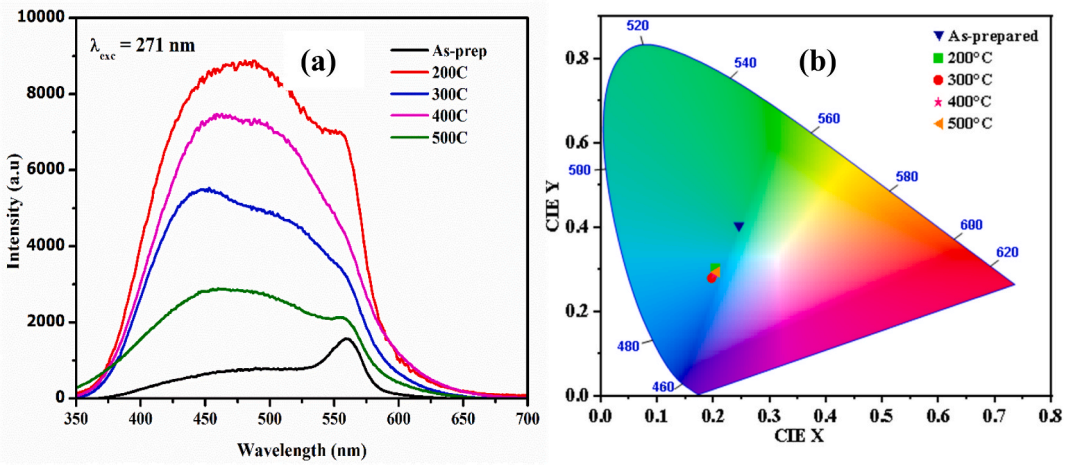

Fig. 7. (a) PL spectra and (b) C.I.E. diagram of as-prepared CdZrS NPs and after annealing sample at indicated temperatures.

Table 1
C.I.E. colour coordinates of the samples.

Samples	As-prepared	200 °C	300 °C	400 °C	500 °C
x-coordinates	0.2417	0.1954	0.1947	0.2025	0.2037
y-coordinates	0.4035	0.2973	0.2781	0.2931	0.2925

dynamics of CdZrS and to design materials with ideals through the integration of computational models and experimental data.

CRediT authorship contribution statement

A.U. Yimamu: Conceptualization, Data curation, Formal analysis, Methodology, Validation, Visualization, Writing – original draft, Writing – review & editing. **V.N. Adoons:** Writing – review & editing, Writing – original draft, Validation, Supervision, Software, Project administration, Methodology, Funding acquisition, Formal analysis, Data curation, Conceptualization. **R.A. Phokojoe:** Conceptualization, Data curation, Formal analysis, Funding acquisition, Writing – original draft, Writing – review & editing.

Data availability

Data will be made available on request.

Declaration of generative AI in scientific writing

No generative AI was used to write this article or part of.

Declaration of competing interest

The authors declare the following financial interests/personal relationships which may be considered as potential competing interests: None. If there are other authors, they declare that they have no known competing financial interests or personal relationships that could have appeared to influence the work reported in this paper.

Acknowledgment

The authors express gratitude to the Department of Chemistry (Qwaqwa campus), and the Department of Physics (Qwaqwa and Bloemfontein), at the University of the Free State for offering facilities for SEM, XRD, (UV–Vis) spectroscopy and PL spectroscopy measurements, respectively.

References

[1] C. De Mello Donegá, Nanoparticles: Workhorses of Nanoscience, vol. 9783662448, 2014, https://doi.org/10.1007/978-3-662-44823-6.
[2] Y. Chen, et al., Structure/property control in photocatalytic organic semiconductor nanocrystals, Adv. Funct. Mater. 31 (36) (2021) 1–37, https://doi.org/10.1002/adfm.202104099.

[3] X. Kong, Y. Yang, H. Zhang, Y.H. Liu, Y. Wang, Advances in II–VI semiconductor magic-size clusters: synthesis, characterization, and applications in nanotechnology, Coord. Chem. Rev. 518 (June) (2024) 216065, https://doi.org/10.1016/j.ccr.2024.216065.

[4] J. Almutlaq, et al., Engineering colloidal semiconductor nanocrystals for quantum information processing, Nat. Nanotechnol. (2024), https://doi.org/10.1038/s41565-024-01606-4.

[5] V. Narasimman, V.S. Nagarethinam, K. Usharani, A.R. Balu, Optoelectronic, magnetic and antibacterial properties of Zr-doped CdS thin films, Optik (Stuttg) 138 (2017) 398–406, https://doi.org/10.1016/j.ijleo.2017.02.099.

[6] R. Woods-Robinson, et al., Wide band gap chalcogenide semiconductors, Chem. Rev. 120 (9) (2020) 4007–4055, https://doi.org/10.1021/acs.chemrev.9b00600.

[7] A. Kuddus, S.K. Mostaque, S. Mouri, J. Hossain, Emerging II-VI wide bandgap semiconductor device technologies, Phys. Scr. 99 (2) (2024), https://doi.org/10.1088/1402-4896/ad1858.

[8] P. Bansal, et al., We Are IntechOpen , the World ' S Leading Publisher of Open Access Books Built by Scientists , for Scientists TOP 1, i, Intech, 2016, p. 15, tourism, https://www.intechopen.com/books/advanced-biometric-technologies/liveness-detection-in-biometrics.

[9] G. Burashev, et al., The superiority of the photocatalytic and antibacterial performance of mechanochemically synthesized CdS nanoparticles over solvothermal-prepared ones, Semicond. Sci. Technol. 39 (4) (2024), https://doi.org/10.1088/1361-6641/ad2b08.

[10] R.K. Sonker, B.C. Yadav, V. Gupta, M. Tomar, Synthesis of CdS nanoparticle by sol-gel method as low temperature NO2 sensor, Mater. Chem. Phys. 239 (August) (2020), https://doi.org/10.1016/j.matchemphys.2019.121975.

[11] R. Demir, S. Okur, M. Şeker, Electrical characterization of CdS nanoparticles for humidity sensing applications, Ind. Eng. Chem. Res. 51 (8) (2012) 3309–3313, https://doi.org/10.1021/ie201509a.

[12] R. Harish, et al., Cytotoxicity assessment of chitosan coated CdS nanoparticles for bio-imaging applications, Appl. Surf. Sci. 499 (2020) 143817, https://doi.org/10.1016/j.apsusc.2019.143817.

[13] C.H. Ashok, K.V. Rao, C.H.S. Chakra, V. Rajendar, Structural properties of CdS nanoparticles for solar cell applications, Int. J. Pure Appl. Sci. Technol. 23 (1) (2014) 8–12.

[14] X. Liu, et al., Hollow CdS-based photocatalysts, J. Mater. 7 (3) (2021) 419–439, https://doi.org/10.1016/j.jmat.2020.10.010.

[15] A.A. Azab, R.S. Ibrahim, R. Seoudi, Investigating the effects of Mn content on the morphology and dielectric properties of CdS nanoparticles, Appl. Phys. Mater. Sci. Process 130 (5) (2024), https://doi.org/10.1007/s00339-024-07426-6.

[16] A. Abdolahzadeh Ziabari, F.E. Ghodsi, Growth, characterization and studying of sol-gel derived CdS nanoscrystalline thin films incorporated in polyethyleneglycol: effects of post-heat treatment, Sol. Energy Mater. Sol. Cells 105 (March) (2012) 249–262, https://doi.org/10.1016/j.solmat.2012.05.014.

[17] Y. Gu, E.S. Kwak, J.L. Lensch, J.E. Allen, T.W. Odom, L.J. Lauhon, Near-field scanning photocurrent microscopy of a nanowire photodetector, Appl. Phys. Lett. 87 (4) (2005) 2005–2007, https://doi.org/10.1063/1.1996851.

[18] E.I. Naik, H.S.B. Naik, R. Viswanath, B.R. Kirthan, M.C. Prabhakara, Effect of zirconium doping on the structural, optical, electrochemical and antibacterial properties of ZnO nanoparticles prepared by sol-gel method, Chem. Data Collect. 29 (2020) 100505, https://doi.org/10.1016/j.cdc.2020.100505.

[19] D.J. Jeejamol, A.M.E. Raj, K. Jayakumari, C. Ravidhas, Optimization of CdO nanoparticles by Zr4+ doping for better photocatalytic activity, J. Mater. Sci. Mater. Electron. 29 (1) (2018) 97–116, https://doi.org/10.1007/s10854-017-7893-3.

[20] R. Bakkiyaraj, M. Balakrishnan, G. Bharath, N. Ponpandian, Facile Synthesis, Structural Characterization, Photocatalytic and Antimicrobial Activities of Zr Doped CeO2 Nanoparticles, vol. 724, Elsevier B.V., 2017, https://doi.org/10.1016/j.jallcom.2017.07.049.

[21] J. Sharma, A. Gupta, O.P. Pandey, Effect of Zr doping and aging on optical and photocatalytic properties of ZnS nanopowder, Ceram. Int. 45 (11) (2019) 13671–13678, https://doi.org/10.1016/j.ceramint.2019.04.061.

[22] A.A. Ibiyemi, et al., Investigating the magnetic domain structure and photonics characters of singled phased hard ferromagnetic ferrite MFe3O4 (M= Co2+, Zn2+, Cd2+) compounds, J. Niger. Soc. Phys. Sci. 6 (1) (2024) 1–12, https://doi.org/10.46481/jnsps.2024.1909.

[23] H.S. Mund, P. Prajapat, S. Dhaka, S. Kumar, A. Saxena, S.S. Meena, Impact of annealing temperature on structural, optical, and Mössbauer properties of nanocrystalline NiFe2O4, J. Mater. Sci. Mater. Electron. 32 (23) (2021) 27232–27242, https://doi.org/10.1007/s10854-021-07089-6.

[24] H.S. Mund, B.L. Ahuja, Structural and magnetic properties of Mg doped cobalt ferrite nano particles prepared by sol-gel method, Mater. Res. Bull. 85 (2017) 228–233, https://doi.org/10.1016/j.materresbull.2016.09.027.

[25] T.K.W. Mohapi, A.U. Yimamu, K.G. Tshabalala, S.J. Motloung, Effect of deposition voltage on the properties of electrodeposited CdZrS thin films for solar cell application, Phys. B Condens. Matter 671 (May) (2023) 415405, https://doi.org/10.1016/j.physb.2023.415405.

[26] K.S. Rahman, et al., Influence of deposition time in CdTe thin film properties grown by Close-Spaced Sublimation (CSS) for photovoltaic application, Results Phys. 14 (May) (2019) 102371, https://doi.org/10.1016/j.rinp.2019.102371.

[27] A.A. Ojo, I.M. Dharmadasa, Factors affecting electroplated semiconductor material properties: the case study of deposition temperature on cadmium telluride, Coatings 9 (6) (2019) 1–15, https://doi.org/10.3390/COATINGS9060370.

[28] S.W. Pawar, et al., "ES Energy & Environment Structural , Morphological and Optical Characterization of Photochemically Deposited Cadmium Selenide Thin Films,", 2022, pp. 106–113.

[29] A.U. Yimamu, M.A. Afrassa, F.B. Dejene, O.K. Echendu, J.J. Terblans, H.C. Swart, The effect of electrolytic solution pH on the properties of electrodeposited CdTe thin films for solar energy application, Opt. Mater. 151 (April) (2024) 115340, https://doi.org/10.1016/j.optmat.2024.115340.

[30] V. Singh, P.K. Sharma, P. Chauhan, Synthesis of CdS nanoparticles with enhanced optical properties, Mater. Charact. 62 (1) (2011) 43–52, https://doi.org/10.1016/j.matchar.2010.10.009.

[31] S. Ktifa, F. Laatar, M. Hassen, N. Yacoubi, H. Ezzaouia, Annealing temperature dependence of structural, optical, and thermal properties of CdSe thin films grown on porous anodic alumina, J. Sol. Gel Sci. Technol. 85 (2) (2018) 340–348, https://doi.org/10.1007/s10971-017-4550-5.

[32] R.B. Kale, C.D. Lokhande, Influence of air annealing on the structural, morphological, optical and electrical properties of chemically deposited ZnSe thin films, Appl. Surf. Sci. 252 (4) (2005) 929–938, https://doi.org/10.1016/j.apsusc.2005.01.154.

[33] D. Lilhare, A. Khare, Development of chalcogenide solar cells: importance of CdS window layer, Opto-Electronics Rev 28 (1) (2020) 43–63, https://doi.org/10.24425/opelre.2020.132500.

[34] F. Gemain, I.C. Robin, S. Renet, S. Bernardi, Photoluminescence studies of CdS layers for solar cells, Phys. Status Solidi Curr. Top. Solid State Phys. 9 (8–9) (2012) 1740–1743, https://doi.org/10.1002/pssc.201100539.

[35] V. Singh, P. Chauhan, Structural and optical characterization of CdS nanoparticles prepared by chemical precipitation method, J. Phys. Chem. Solids 70 (7) (2009) 1074–1079, https://doi.org/10.1016/j.jpcs.2009.05.024.

[36] J.I. Contreras-Rascón, J. Díaz-Reyes, A. Flores-Pacheco, R. Lozada Morales, M.E. Álvarez-Ramos, J.A. Balderas-López, Structural and optical modifications of CdS properties in CdS-Au thin films prepared by CBD, Results Phys. 22 (February) (2021), https://doi.org/10.1016/j.rinp.2021.103914.

[37] R.A. Phokojoe, S.V. Motloung, T.E. Motaung, M.A. Kebede, H.C. Swart, L.F. Koao, Effect of annealing time on copper selenide thin films prepared by chemical bath deposition, Phys. B Condens. Matter 666 (June) (2023) 415112, https://doi.org/10.1016/j.physb.2023.415112.